Corrosion Science 106 (2016) 298–302

Corrosion Science

journal homepage: www.elsevier.com/locate/corsci

Short communication

Simultaneous visualization of pH and Cl^- distributions inside the crevice of stainless steel

Masashi Nishimoto*, Junichiro Ogawa[1], Izumi Muto*, Yu Sugawara, Nobuyoshi Hara

Department of Materials Science, Tohoku University, Aoba-ku, Sendai 980-8579, Japan

ARTICLE INFO

Article history:
Received 6 November 2015
Received in revised form 25 January 2016
Accepted 28 January 2016
Available online 1 February 2016

Keywords:
A. Stainless steel
B. Potentiostatic
C. Crevice corrosion

ABSTRACT

A sensing plate for the simultaneous measurements of pH and Cl^- concentration was fabricated. Terbium–dipicolinic acid complex (Tb–DPA) and quinine sulphate were used to measure the pH and Cl^- concentration, respectively. In the incubation period of the crevice corrosion, the pH inside the crevice gradually decreased from 3.0 to *ca.* 2.0, and the Cl^- concentration increases from 0.01 to *ca.* 0.18 M. The generation of the micro-pit led to a sharp decrease in pH to below 0.5 and an increase in the Cl^- concentration to above 4 M. This situation allowed the crevice corrosion to proceed without spontaneously stopping.

1. Introduction

Understanding the corrosion mechanisms of metals is of substantial interest in engineering because corrosion causes considerable economic loss due to the structural failure of critical components in infrastructure. Localized corrosion, such as pitting and crevice corrosion, is complicated by the synergistic effect of H^+ and Cl^- ions on metal dissolution [1–6]. Full elucidation of the mechanisms of localized corrosion requires simultaneous measurements of the H^+ and Cl^- distributions. Chemical imaging is a technique that provides the spatial distribution of chemical species at metal/solution interfaces, and fluorescence dyes are widely used in this application [7,8]. Rare-earth complexes are well known to enable pH imaging [9–11]. Trout et al. demonstrated that the terbium–dipicolinic acid complex (Tb–DPA) can be used for pH measurements between *ca.* pH 2 and 4 [9]. However, pH imaging in corrosive environments has not been intensively studied because fluorescence is quenched in low-pH and/or highly concentrated Cl^- solutions. In corrosion reactions, the hydrolysis reaction of dissolving metal ions causes severe acidification and Cl^- accumulation (*e.g.*, pH < 1 and Cl^- > 1 M). Although Cl^--sensitive fluorescence dyes such as 6-methoxy-*N*-(3-sulfopropyl)quinolinium (SPQ) and *N*-(ethoxycarbonylmethyl)-6-methoxyquinolinium bromide (MQAE) have been successively applied to imaging in the field of biology [12–14], their sensitivity tends to be insufficient for corrosion research. Kaji et al. observed that quinine sulphate is suitable for Cl^- imaging and developed a Cl^- sensing plate that can be used in highly concentrated Cl^- solutions [15]. However, research on the simultaneous measurements of pH and Cl^- concentration is still developing. The objectives of this study were to fabricate a sensing plate for simultaneous measurements of pH and Cl^- concentration and to analyse the changes in the pH and Cl^- distributions during the crevice corrosion of stainless steel. Simultaneous visualization techniques for pH and Cl^- distributions offer great advantages over other techniques in the challenge to understand not just the corrosion mechanisms but also other chemical reactions in aqueous solutions.

2. Experimental

2.1. pH$^-$ and Cl$^-$-sensitive fluorescent dyes

To fabricate the sensing plate for the simultaneous measurements of pH and Cl^- concentration, Tb–DPA and quinine sulphate as the fluorescent dyes were chosen. Tb–DPA was used as the sensing dye for the pH measurements, and quinine sulphate was used to measure the Cl^- concentration. Tb–DPA was formed by mixing $Tb_2(SO_4)_3$ and dipicolinic acid. The excitation and emission spectra of Tb–DPA and quinine sulphate in the mixtures of dilute H_2SO_4 and

* Corresponding authors. Fax: +81 22 795 7299.
E-mail addresses: masashi.nishimoto.s5@dc.tohoku.ac.jp (M. Nishimoto), mutoi@material.tohoku.ac.jp (I. Muto).
[1] Present address: Fuji Heavy Industries, Ltd., Mitaka City, Tokyo 181-8577, Japan.

http://dx.doi.org/10.1016/j.corsci.2016.01.028
0010-938X/

NaCl solutions were collected using a JASCO FP-6200 spectrophotometer.

2.2. Fabrication of sensing plate

To fabricate the sensing plate for simultaneous measurements of pH and Cl^- concentration, we used the sol–gel method to deposit the sensing layer, which contained two fluorescent dyes, onto one side of a glass plate. A mixture of pure water (80 mL), polyvinyl alcohol (0.5 g), 0.01 M NaOH (20 mL), dipicolinic acid (0.172 g), $Tb_2(SO_4)_3$ (0.125 g), and quinine sulphate (0.05 g) was prepared (solution A). Then, a mixture of tetramethyl orthosilicate (2 mL), 0.05 M H_2SO_4 (1 mL), and ethanol (1 mL) was stirred for 10 min. Afterwards, 2 mL of solution A was added, and the mixture was stirred for 20 min. Finally, the mixture was spin-coated onto a silica glass plate (1 mm thick) and dried at room temperature. The glass plate with the sol–gel layer was stored in solution A excluding polyvinyl alcohol to prevent cracking of the sensing layer.

2.3. Validation of sensing plate

The mixed solutions of H_2SO_4 and NaCl as standards for the pH and Cl^- concentrations were used. The Cl^- concentrations were 0.01, 0.1, 1, and 4 M, and the pH was adjusted to 0.5, 1.0, 2.0, and 3.0. To validate the colour change of the sensing plate, a thin layer of the standard solution was formed on a mirror-polished Pt plate, and then the sensing plate was placed on the thin layer. Next, fluorescence micrographs were collected using an Olympus BX51 microscope equipped with an UPlanFL ×4/0.13 air objective and a DP71 CCD camera system. For pH validation, the excitation filter was set at 270 nm and a 475–570 nm band-pass filter composed of low-pass and high-pass filters was used to detect the fluorescence of Tb–DPA. For the validation of the Cl^- concentration, the wavelength of the excitation filter was changed to 330 nm to excite only quinine sulphate and a 380–530 nm band-pass filter was used to detect its fluorescence. All micrographs were saved in the JPEG format. After the experiments, the images were converted into the BMP format, and the RGB values in each pixel were extracted.

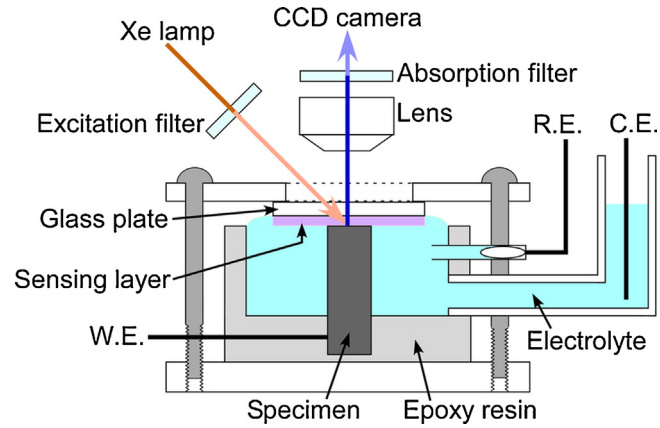

Fig. 1. Schematic of the crevice corrosion test apparatus.

2.4. Crevice corrosion test

To analyse the initiation process in the crevice corrosion of stainless steels, we used the sensing plate as a crevice former and conducted simultaneous measurements of pH and Cl^- concentration inside the crevice (Fig. 1). A high-manganese austenitic stainless steel (Fe–18Cr–10Ni–5.4Mn) was used as the specimen. This steel was heat-treated at 1373 K for 30 min and then quenched in water. After the heat-treatment, the steel was cut into pieces with dimensions of 3 mm × 3 mm × 18 mm and all of the surfaces of the cut pieces were polished diamond paste down to 1 μm. The specimen was passivated in 30% HNO_3 at 323 K for 30 min. Afterwards, the lower part of the specimen was embedded in epoxy resin. The upper surface of the specimen was then polished again with 1 μm diamond paste. The specimen was polarized at 0.4 V (vs. Ag/AgCl, 3.33 M KCl) in naturally aerated 0.01 M NaCl (pH 3.0, adjusted with 0.01 M HCl) at 298 K. All the electric potentials reported in this work refer to an Ag/AgCl (3.33 M KCl) electrode.

Optical and fluorescence micrographs were collected at constant intervals during the crevice corrosion tests. These micrographs could not be collected at precisely the same time. In our

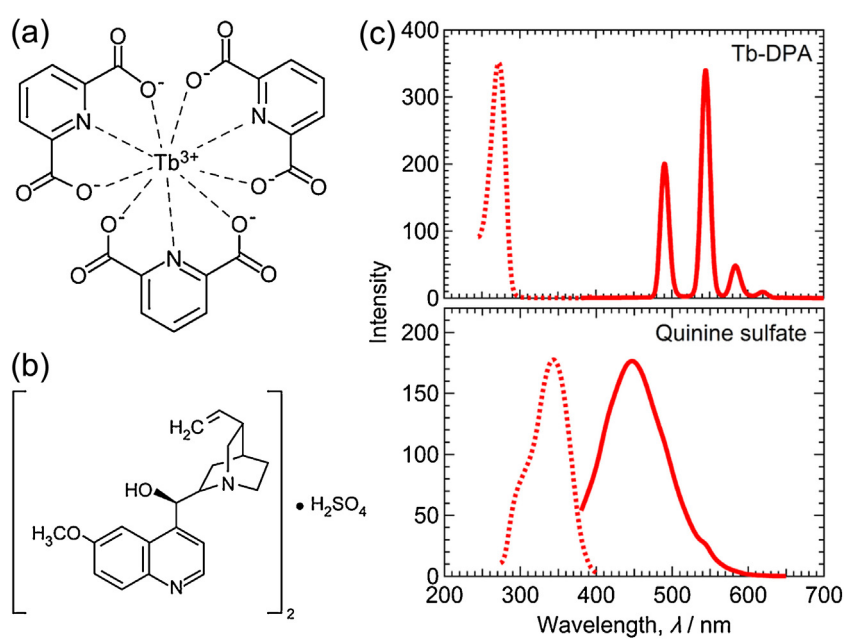

Fig. 2. Molecular structure of (a) Tb–DPA and (b) quinine sulphate. (c) Excitation (- - -), and emission (—) spectra of Tb–DPA and quinine sulphate in 0.01 M NaCl at pH 3.0 (adjusted with H_2SO_4).

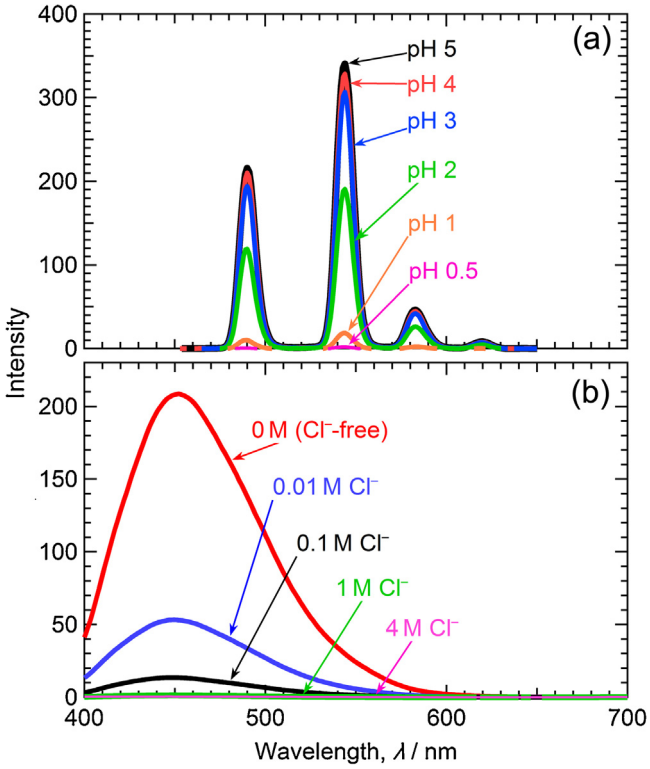

Fig. 3. (a) Emission spectra of Tb–DPA in 1 M Cl^- solutions at pH 5, 4, 3, 2, 1, and 0.5. (b) Emission spectra of quinine sulphate in pH 3.0 solutions at 0 M (Cl^--free), 0.01 M, 0.1 M, 1 M, and 4 M Cl^-.

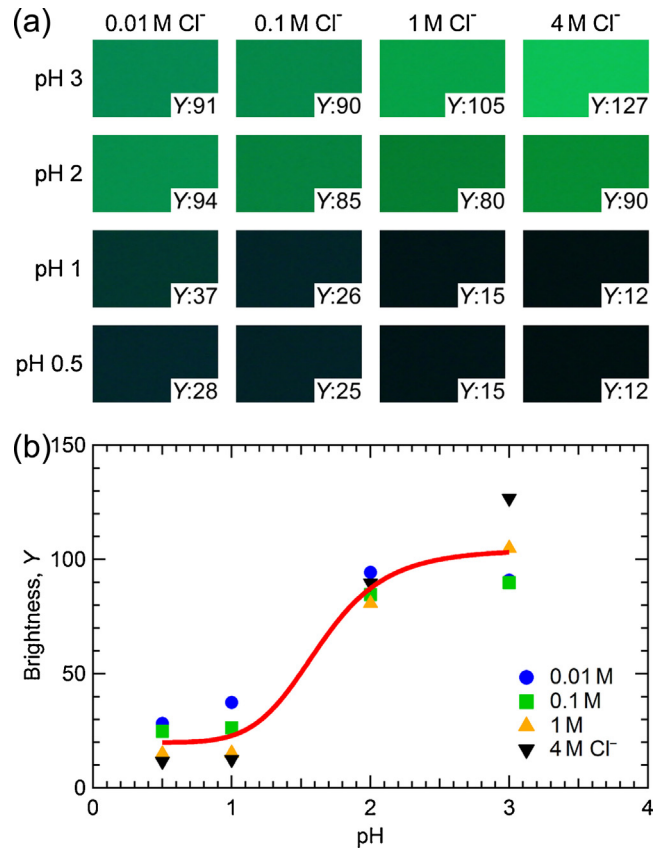

Fig. 4. (a) Fluorescence micrographs of the sensing plate and (b) the relationship between pH and the brightness parameter Y of a sensing plate placed on the Pt surface covered with a solution layer at various pH and Cl^- concentrations. Brightness parameter: $Y = 0.299R + 0.587G + 0.114B$.

system, approximately 17 s is required to exchange the filters, store the image data, and reconfigure the exposure time.

3. Results and discussion

3.1. Fluorescence properties of Tb–DPA and quinine sulphate

The excitation spectrum of Tb–DPA (Fig. 2a) exhibits a peak at 272 nm, and the emission spectrum shows four bands with a maximum at 544 nm (green fluorescence) (Fig. 2c). This large Stokes shift is a characteristic feature in the fluorescence of rare-earth complexes [16]. Quinine sulphate (Fig. 2b) exhibits blue fluorescence, as indicated in Fig. 2c. The peak wavelengths of the excitation and emission are 343 nm and 447 nm, respectively. These maximum wavelengths differ from those of Tb–DPA. Therefore, quinine sulphate and Tb–DPA can be excited independently by changing the wavelength of a band-pass filter for a Xe-lamp, and their emission fluorescence can be recorded separately. Strictly speaking, quinine sulphate is slightly excited in the case of the Tb–DPA excitation at 270 nm because the excitation wavelength for quinine sulphate is longer than that for Tb–DPA; however, the fluorescence from quinine sulphate is eliminated by an absorption filter. The fluorescence of Tb–DPA and quinine sulphate is therefore detected with little interference on each other.

To ascertain the effects of pH and Cl^- concentration on the fluorescence intensity of these dyes, we acquired the emission spectra of Tb–DPA in dilute H_2SO_4 at pH from 5.0 to 0.5 (1 M Cl^-) and those of quinine sulphate in NaCl solutions (pH 3.0) containing Cl^- at concentrations from 0 to 4 M. As shown in Fig. 3, the fluorescence intensity of Tb–DPA decreases with decreasing pH and the intensity of the emission spectra of quinine sulphate decreases with increasing Cl^- concentration.

3.2. Performance of sensing plate

As shown in Fig. 4a, the green fluorescence of Tb–DPA decreases with decreasing pH and is independent of the Cl^- concentration. The *RGB* values in each pixel of the images were extracted and converted into the brightness parameter Y by the following expression:

$$Y = 0.229R + 0.587G + 0.114B$$

The brightness Y decreases with decreasing pH (Fig. 4b). A small influence of the Cl^- concentration on the brightness was observed because of the overlapping emission spectra of Tb–DPA and quinine sulphate. Nonetheless, we still estimated the pH of the solution on the metal surfaces.

As evident in Fig. 5, the intensity of the blue fluorescence of quinine sulphate decreases with increasing Cl^- concentration and is independent of pH. In addition, a quantitative relationship between the Cl^- concentration and the brightness Y is observed, which allows the Cl^- concentration in solutions to be measured. The sensing plate for the simultaneous measurements of pH and Cl^- concentration using Tb–DPA and quinine sulphate were successfully fabricated.

3.3. Changes in pH and Cl^- distributions in crevice solution

Fig. 6a shows the optical micrograph of the inside of the crevice after the crevice corrosion test. Crevice corrosion was generated in the area indicated by a white rectangle. The corroded area was observed using a JSM-7100F scanning electron microscope. As shown in Fig. 6b, a micro-pit was observed; we assumed that

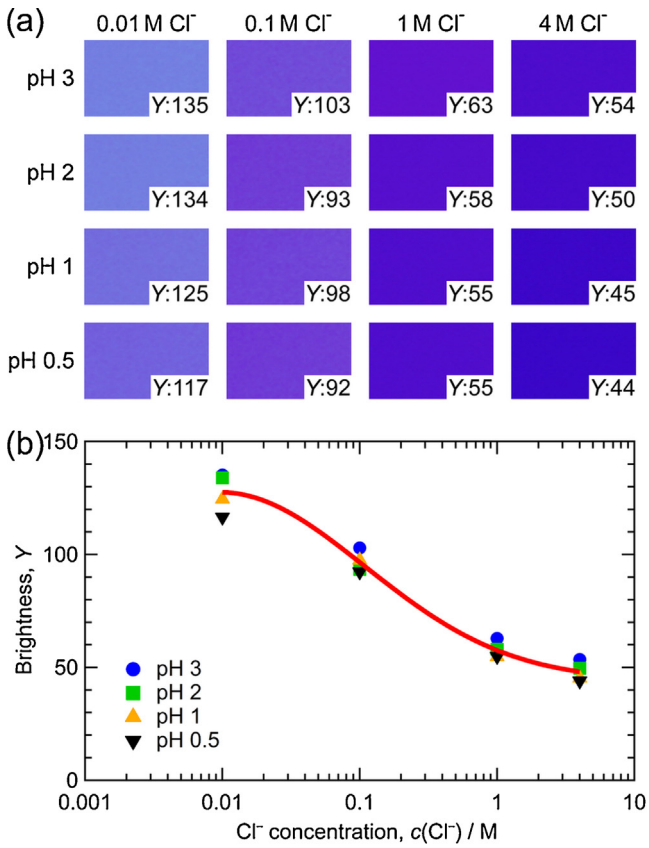

Fig. 5. (a) Fluorescent micrographs of the sensing plate and (b) the relationship between the Cl^- concentration and the brightness parameter Y of a sensing plate placed on the Pt surface covered with a solution layer at various pH and Cl^- concentrations. Brightness parameter: $Y = 0.299R + 0.587G + 0.114B$.

crevice corrosion was initiated here as pitting corrosion. Fig. 6c shows the optical and fluorescence micrographs of the pH and Cl^- sensing plate in the area indicated by the white rectangle in Fig. 6a. The crevice mouth was located at the bottom of the micrographs, and some defects were present on the surface of the sensing plate, which were likely generated during the spin-coating process. From the beginning of the corrosion test to 1347 s, the brightness of the fluorescence micrographs for both pH and Cl^- gradually decreased with time, indicating that both acidification and Cl^- accumulation occurred. At approximately 1340 s, the pH inside the crevice reached *ca.* 2.0 and the Cl^- concentration became *ca.* 0.18 M (Fig. 7).

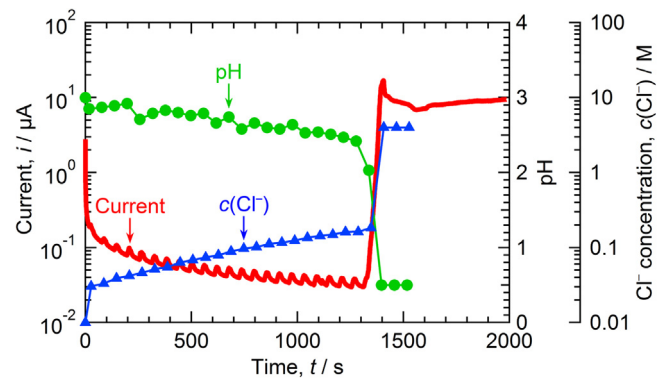

Fig. 7. Time variations of the total current, the pH, and the Cl^- concentration at the initiation site of crevice corrosion on 18Cr–10Ni–5.4Mn austenitic stainless steel polarized at 0.4 V in 0.01 M NaCl (pH 3.0, adjusted with 0.01 M HCl).

The gradual decrease in pH inside the crevice was likely due to the hydrolysis reaction of metal ions dissolved from the steel surface, and the Cl^- accumulation maintained electrical neutrality inside the crevice. This study clearly confirms that the electromigration of Cl^- ions occurs towards the inside of the crevice from the outside during crevice corrosion and that the acidification of the crevice solution proceeds simultaneously.

At 1380 s, a very small black spot appeared at the position marked by the arrow in Fig. 6c, and its position is consistent with that of the pit shown in Fig. 6b. This result suggests that the black spot corresponds to the initiation site of crevice corrosion and that the initial morphology of the crevice corrosion is pitting. Immediately after the crevice corrosion initiation, the dark area suddenly spread in both fluorescence micrographs. The pH and Cl^- concentration inside the dark area are estimated to be below pH 0.5 and above 4 M Cl^-, respectively. Fig. 7 shows the time variations of the total current, the pH and the Cl^- concentration at the initiation site of crevice corrosion. From 0 to 1347 s, the pH inside the crevice gradually decreases from 3.0 to *ca.* 2.0, and the Cl^- concentration increases from 0.01 to *ca.* 0.18 M. This period is considered the incubation period of crevice corrosion. During this period, the dissolution rate of the steel is low because the steel surface is initially passive. The hydrolysis reaction of dissolving metal ions causes weak acidification inside the crevice, and the gradual accumulation of Cl^- maintains electrical neutrality. The generation of the micro-pit inside the crevice leads to a sharp decrease in pH to below 0.5 and an increase in the Cl^- concentration to above 4 M. The release of a large amount of metal ions over a short time as pitting occurs results in a large decrease in pH around the pit due

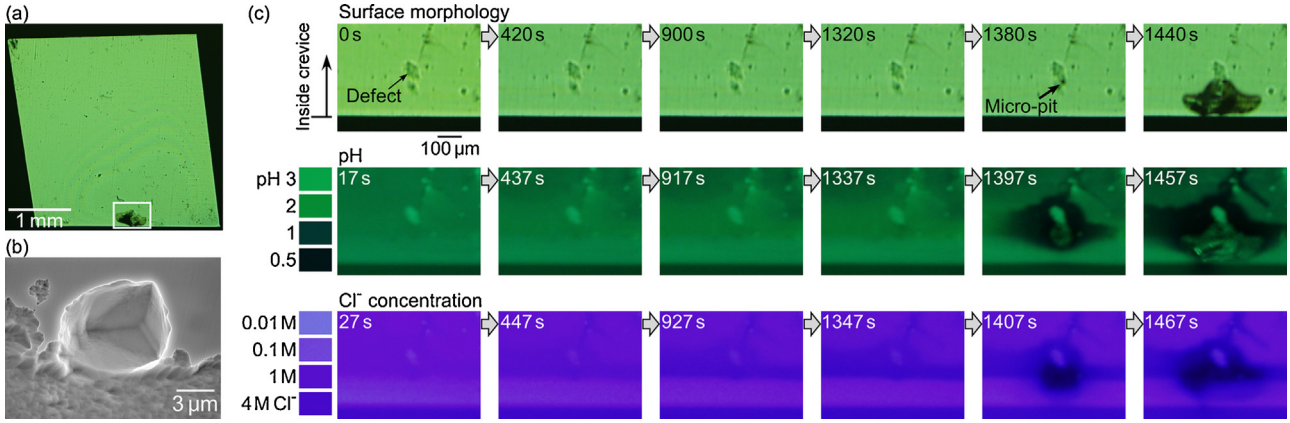

Fig. 6. (a) Optical micrograph of the upper surface of the specimen at the end of the crevice corrosion test. (b) SEM image of the micro-pit at the initiation site of the crevice corrosion. (c) The optical and fluorescence micrographs of the sensing plate were collected in the area indicated by the white rectangle in (a).

to the hydrolysis reaction. Moreover, an increase in the accumulation of Cl^- occurs inside the crevice as a result of electromigration. The increased acidification and Cl^- accumulation provide a local solution environment that allows the crevice corrosion to proceed without spontaneously stopping. Crevice corrosion grows rapidly after this initiation period.

4. Conclusions

1. A sensing plate for use in the simultaneous measurements of pH and Cl^- concentration was successfully fabricated. Terbium–dipicolinic acid complex (Tb–DPA) was used as the sensing dye for the pH measurements, and quinine sulphate was used to measure the Cl^- concentration. It was confirmed that the changes in the pH and Cl^- concentration of the solution was estimated quantitatively from the colour of the sensing plate.
2. The changes in the pH and Cl^- distributions during the crevice corrosion of 18Cr–10Ni–5.4Mn stainless steel were elucidated. In the incubation period of the crevice corrosion, the pH inside the crevice gradually decreased from 3.0 to *ca.* 2.0, and the Cl^- concentration increased from 0.01 to *ca.* 0.18 M. The generation of the micro-pit inside the crevice led to a sharp decrease in pH to below 0.5 and an increase in the Cl^- concentration to above 4 M. This situation allowed the crevice corrosion to proceed without spontaneously stopping.

Acknowledgement

This work was supported by a Grant-in-Aid for Scientific Research B (KAKENHI) from the Japan Society for the Promotion of Science, grant No. 25289257.

References

[1] P. Combrade, Crevice corrosion of metallic materials, in: P. Marcus (Ed.), Corrosion Mechanisms in Theory and Practice, 3rd ed., CRC Press, Boca Raton, 2011, pp. 449–498.
[2] J. Mankowski, Z. Szklarska-Smialowska, Studies on accumulation of chloride ions in pits growing during anodic polarization, Corros. Sci. 15 (1975) 493–501.
[3] A. Alavi, R.A. Cottis, The determination of pH, potential and chloride concentration in corroding crevices on 304 stainless steel and 7475 aluminium alloy, Corros. Sci. 27 (1987) 443–451.
[4] K. Cho, H.W. Pickering, The role of chloride ions in the IR > IR* criterion for crevice corrosion in iron, J. Electrochem. Soc. 138 (1991) L56–L58.
[5] P.C. Pistorius, G.T. Burstein, Aspects of the effects of electrolyte composition on the occurrence of metastable pitting on stainless steel, Corros. Sci. 36 (1994) 525–538.
[6] R.C. Wolfe, K.G. Weil, B.A. Shaw, H.W. Pickering, Measurement of pH gradients in the crevice corrosion of iron using a palladium hydride microelectrode, J. Electrochem. Soc. 152 (2005) B82–B88.
[7] A. Picot, A. D'Aléo, P.L. Baldeck, A. Grichine, A. Duperray, C. Andraud, O. Maury, Long-lived two-photon excited luminescence of water-soluble europium complex: applications in biological imaging using two-photon scanning microscopy, J. Am. Chem. Soc. 130 (2008) 1532–1533.
[8] M.H. Lee, N. Park, C. Yi, J.H. Han, J.H. Hong, K.P. Kim, D.H. Kang, J.L. Sessler, C. Kang, J.S. Kim, Mitochondria-immobilized pH-sensitive off–on fluorescent probe, J. Am. Chem. Soc. 136 (2014) 14136–14142.
[9] T.K. Trout, J.M. Bellama, R.A. Faltynek, E.J. Parks, F.E. Brinckman, Effect of pH on the emission properties of aqueous tris(2,6-dipicolinato) terbium(III) complexes, Inorg. Chim. Acta 155 (1989) 13–15.
[10] N. Takahashi, S. Saito, H. Hoshino, Formation reactions and photophysical parameters of highly luminescent lanthanoids(III) complexes with 4-hydroxypyridine-2,6-dicarboxylic acid, Bunseki Kagaku 52 (2003) 713–718.
[11] T. Gunnlaugsson, J.P. Leonard, K. Sénéchal, A.J. Harte, pH responsive Eu(III)–phenanthroline supramolecular conjugate: novel off–on–off luminescent signaling in the physiological pH range, J. Am. Chem. Soc. 125 (2003) 12062–12063.
[12] J.E. O'Reilly, Fluorescence experiments with quinine, J. Chem. Educ. 52 (1975) 610–612.
[13] A.S. Verkman, Development and biological applications of chloride-sensitive fluorescent indicators, Am. J. Physiol. Cell Physiol. 259 (1990) C375–C388.
[14] A. Ma, Z. Rosenzweig, Submicrometric lipobead-based fluorescence sensors for chloride ion measurements in aqueous solution, Anal. Chem. 76 (2004) 569–575.
[15] T. Kaji, T. Sekiai, I. Muto, Y. Sugawara, N. Hara, Visualization of pH and pCl distributions: initiation and propagation criteria for crevice corrosion of stainless steel, J. Electrochem. Soc. 159 (2012) C289–C297.
[16] J.-C.G. Bünzli, Lanthanide luminescence for biomedical analyses and imaging, Chem. Rev. 110 (2010) 2729–2755.